



Supplement of

Increase in precipitation scavenging contributes to long-term reductions of light-absorbing aerosol in the Arctic

Dominic Heslin-Rees et al.

Correspondence to: Dominic Heslin-Rees (dominic.heslin-rees@aces.su.se) and Radovan Krejci (radovan.krejci@aces.su.se)

The copyright of individual parts of the supplement might differ from the article licence.

S1 Data availability

Figure S1 shows the available data used in this study and periods in which the instruments overlap and intercomparisons between the measurements can be made.

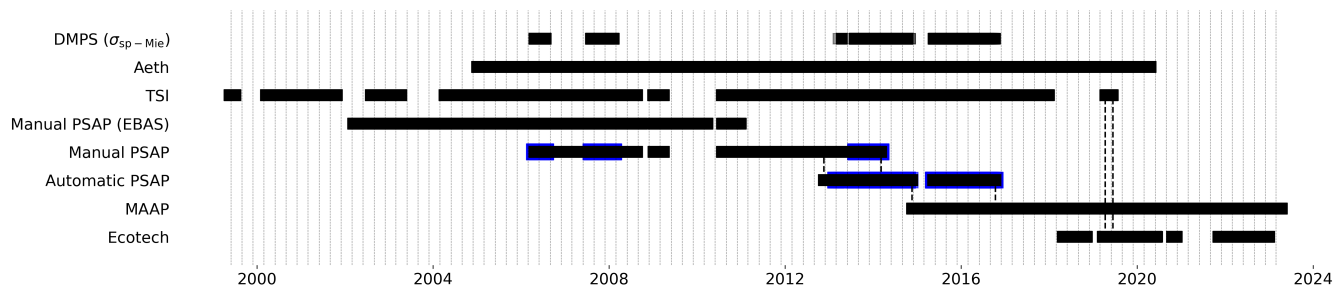


Figure S1. Data availability: the data deemed usable and valid are presented as a horizontal line plot. Each instrument or dataset is labelled accordingly. Note that PSAP (EBAS) corresponds to the absorption coefficient downloaded from the EBAS database (<https://ebas.nilu.no/>), it is the same instrument (i.e. the manual PSAP) however the data has been processed slightly differently. The variables taken from each data set are as follows absorption coefficient at 660 nm from the Aethalometer (Aeth), converted to 637, scattering coefficient at 550 nm from the TSI nephelometer (TSI), absorption coefficient at 525 nm from the manual PSAP (Manual PSAP EBAS), absorption coefficient at 525 nm from the manual PSAP (manual PSAP), absorption coefficient at 525 nm from the automatic PSAP (automatic PSAP), absorption coefficient at 637 nm from the Multi-Angle Absorption Photometer (MAAP), and the scattering coefficient at 525 nm from the Ecotech nephelometer (Ecotech). Missing data, when the instrument experienced problems or was away for servicing, are displayed as gaps in the line plot. All the instruments used in this study are presented and the periods in which intercomparisons were performed are signalled by the space between the dashed vertical lines. The MAAP and the automatic PSAP overlapped during the period between the 19th of November 2014 to the 13th of October 2016. The manual PSAP and the automatic PSAP overlapped between 19th of November 2012 to 21st March 2013. The blue around the manual and automatic PSAP correspond to the additional hourly values brought about by including the DMPS-derived Mie scattering coefficient data.

S2 Harmonisation

5 S2.1 Treatment of PSAPs

For the “automatic PSAP” and “manual PSAP”, each filter was plotted separately, so that intensity (I) and volume (Q) could be visually inspected. In general, I , monotonically decreases over time as aerosol particles, in particular light-absorbing aerosols, settle on the filters. A threshold of 0.5 for the ratio between the measured transmittance and initial transmittance (τ) is set for when the exposed filter surface was changed; the build-up of aerosol particles can cause artefacts and hence the ratio cannot be too low. The σ_{ap} is then calculated based on the Bond correction scheme (see eq. S.1), using a time step of 15 minutes for the “manual PSAP” and “automatic PSAP”. The Bond correction scheme accounts for the influence of scattering particles via the SSA (single-scattering albedo). The light scattering coefficient (σ_{sp}) is provided by the Nephelometer. For periods in which nephelometer measurements were invalid or not present, Mie-derived scattering from the aerosol size distribution measured by a Differential Mobility Particle Sizer (DMPS) at Zeppelin station was used to estimate σ_{sp} (with an assumed refractive index of $m = 1.544+0i$). It is understood there are substantial uncertainties, however, for the purposes of simply correcting the PSAP measurements, the use of the DMPS-derived Mie scattering is considered acceptable (Zieger et al., 2010).

Bond et al. (1999) describes these corrections in detail. It should be added that no flow corrections, nor spot size corrections were applied to the data. The formula for the Bond correction is as follows:

$$\sigma_{ap}(t) = \frac{A}{Q \cdot \Delta t} \ln\left(\frac{I(t - \Delta t)}{I(t)}\right) \cdot \frac{1}{1.37 \cdot \tau + 0.866} - 0.016 \cdot \sigma_{sp}, \quad (S.1)$$

20 where σ_{ap} is the absorption coefficient, A is the Area of the sample spot/filter area [m^2], Q is the flow rate [given in litres per minute, but converted to m^3 /minute], Δt is the time step used for integrating the measurements (i.e., 15 mins), $I(t-\Delta t)$ is the filter transmittance at time, $t-\Delta t$, and $I(t)$ is the filter transmittance at time, t . τ is the filter transmission (i.e. I/I_0) and σ_{sp} is the scattering coefficient.

It should be noted that the automatic PSAP initially showed instability, with strong fluctuations in I/I_0 , however, a resolution of 1 hour applied to data processed with a running mean of 20 minutes resolves the issue. It is likely that the observed increase in noise is the result of large fluctuations in the sample flow due to an improper trigger algorithm to set the sample flow.

Prior to 2006-04-20, σ_{ap} is acquired from EBAS (<http://ebas.nilu.no/>, last access: 07 01 2022). The σ_{ap} from EBAS is from the manual PSAP, however, slightly different post-processing has been performed.

All hourly σ_{ap} mean values greater than 0 Mm^{-1} were considered valid.

30 S2.2 Treatment of MAAP data

The MAAP operates at a constant flow rate of 1000 L hr^{-1} , and data was deemed invalid if the flow rate decreased below 900 L hr^{-1} . It is assumed that the NOAA software does most of the interpretation internally and just outputs a missing value code if the data is affected. The NOAA software additionally converts the parameters to STP (as signified by the 0x0200 system flag). All erroneous data were removed before taking hourly arithmetic means. The MAAP operated at a resolution of around 1-2 minutes.

Only values greater than 0 Mm^{-1} were considered valid. This is despite the stated detection limit by the manufacturers, for a 30-minute time resolution, being approximately $<0.13 \text{ Mm}^{-1}$ (or 20 ng m^{-3}).

S2.3 Harmonisation

The time series for the σ_{ap} measurements is composed of different instruments which have each respectively undergone several changes (e.g., maintenance and calibration). Therefore, it is important to show the temporal evolution of these changes in relation to the other instruments.

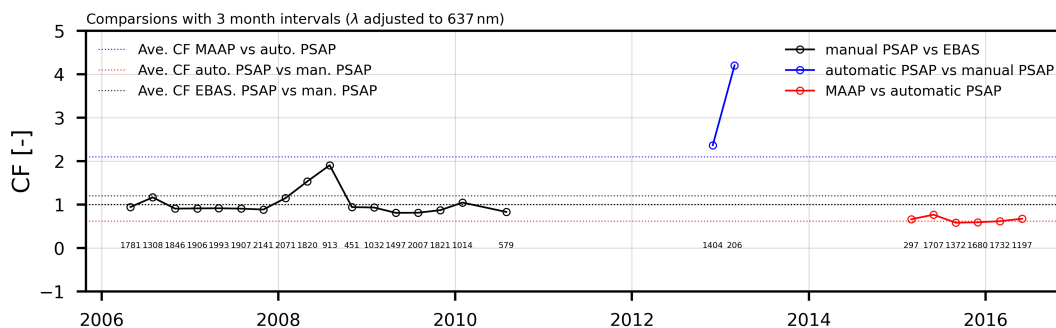


Figure S2. Harmonisation timeline: data from the different instruments are compared with one another to ascertain the coefficient of regression (using the Theil Sen Slope). The reciprocal is the correction factor (CF). In total, three comparisons are performed namely, 1. (in black) absorption coefficient (σ_{ap}) from the EBAS database (based on the custom-built manual Particle Soot Absorption Photometer (PSAP)) vs. the σ_{ap} from the same manual custom-built PSAP, 2. (in blue) σ_{ap} from the automatic PSAP vs. σ_{ap} from the manual PSAP, and 3. (in red) σ_{ap} from the Multi-Angle Absorption Photometer (MAAP) vs. σ_{ap} from the automatic PSAP. Comparisons are done for every 3-month interval. All σ_{ap} are given at the wavelength 637 nm. The number of data points for each comparison is represented in the integer value below the line plots. EBAS refers to the database infrastructure operated by the Norwegian Institute for Air Research (NILU) (<https://ebas.nilu.no/>). The data taken from EBAS was the absorption coefficient from the same custom-built PSAP instrument. It should in theory correspond identically to the values processed in this manuscript, however, there were slightly different approaches to the handling of the PSAP data, and as such the correction factors are not 1:1.

Figure S2 describes the evolution of the correction factor (CF) for the comparisons of the various instruments. In Fig S2, the first comparison compares the absorption coefficient (σ_{ap}) produced in this study (i.e. manual PSAP) and the σ_{ap} data produced and uploaded to EBAS from the same instrument (i.e. EBAS PSAP). It is clear that for the majority of the σ_{ap} data, there is a 1:1 correspondence. The slight discrepancies between the two data sets could be the result of the different scattering coefficients used in the correction, or the different averaging used. The second comparison (blue line) refers to the σ_{ap} data derived from the automatic PSAP compared to the σ_{ap} data derived from the manual PSAP. For this comparison, there is a significant shift in the two data sets, from σ_{ap} derived from the automatic PSAP from 2 to over 4 times greater than the σ_{ap} from the manual PSAP. Despite, this 3-month period where the automatic PSAP exhibited values 4 times greater than the manual PSAP, an average of 2.11 is considered to represent the relation between the two instruments. Lastly, the comparison between the MAAP and automatic PSAP (red line) shows a relatively stable relation, with a semi-constant correction factor. The MAAP values correspond to values slightly lower than the automatic PSAP values.

Using the comparison between the MAAP and the automatic PSAP, a correction factor (CF) of 0.61 was ascertained. Hence, the measurements from the automatic PSAP were multiplied by the CF of 0.61. After this, the measurements from the automatic PSAP with the CF=0.61 applied were compared to the manual PSAP; a value of 1.30 was applied to the manual PSAP. Finally, a CF of 1.20 was applied to the absorption coefficient data set taken from the EBAS database (<https://ebas-data.nilu.no/>). Despite the fact that both the EBAS data set and the data processed here in this manuscript are taken from the same instrument (i.e. the custom-built PSAP), the values are not identical (i.e. a CF of 1 for all time points). The reason for the scatter, as mentioned above as well, can be related to small differences in any of the variables that enter the calculations. The aforementioned correction factors are applied in the correct order to various time periods to produce the harmonised full-time series.

For the comparisons to be done using the same operational wavelengths, the σ_{ap} measured and recorded by the PSAPs was converted from 525 nm (wavelength the PSAP operates on) to 637 nm. The conversion was done by assuming an Absorbing Ångström Exponent (ÅAE) of 1 (i.e. pure EC) (see Eq.S.2). Examining the ÅAE from the Aethalometer data this was considered a fair assumption (see Section). The equation for converting σ_{ap} from one wavelength to another is given as follows:

$$\sigma_{ap}^{\lambda_2} = \sigma_{ap}^{\lambda_1} \left(\frac{\lambda_1}{\lambda_2} \right)^{AAE}, \quad (S.2)$$

where λ_1 and λ_2 are the wavelengths, and AAE is the Absorbing Ångström Exponent. This utilises the $1/\lambda$ dependence and is based on the “small particle limit” theory (Hulst and van de Hulst, 1981) and hence to adjust for example from 525 nm to 637 nm, $\sigma_{ap}^{637} = \sigma_{ap}^{525} (525/637)$ is used.

The Theil-Sen slope estimator (TS) was used to calculate the gradient of the slope for each comparison; for robustness, a simple least-mean-squares approach (LMS) was also utilised, however, the CF was determined based on the TS result. For the intercomparisons only values between 0 - 3.5 Mm^{-1} were used, so that extreme values did not affect the intercomparisons too much. The correction factors are applied to the data as follows:

$$\sigma_{ap,CF}^{637} = \frac{\sigma_{ap,uncor.}^{637}}{CF}, \quad (S.3)$$

where $\sigma_{ap,CF}^{637}$ is the corrected absorption coefficient (i.e. relative to the value from the MAAP), CF is the correction factor and $\sigma_{ap,uncor.}^{637}$ simply represents the uncorrected data.

It should be noted that the most significant source of uncertainty for the PSAP measurements arises from the choice of a correction scheme (e.g., Bond et al., 1999; Virkkula, 2010; Ogren, 2010). In this study, the PSAP measurements are compared with the MAAP measurements, and hence any uncertainties related to the choice of the correction scheme are embedded in the CF applied to the data.

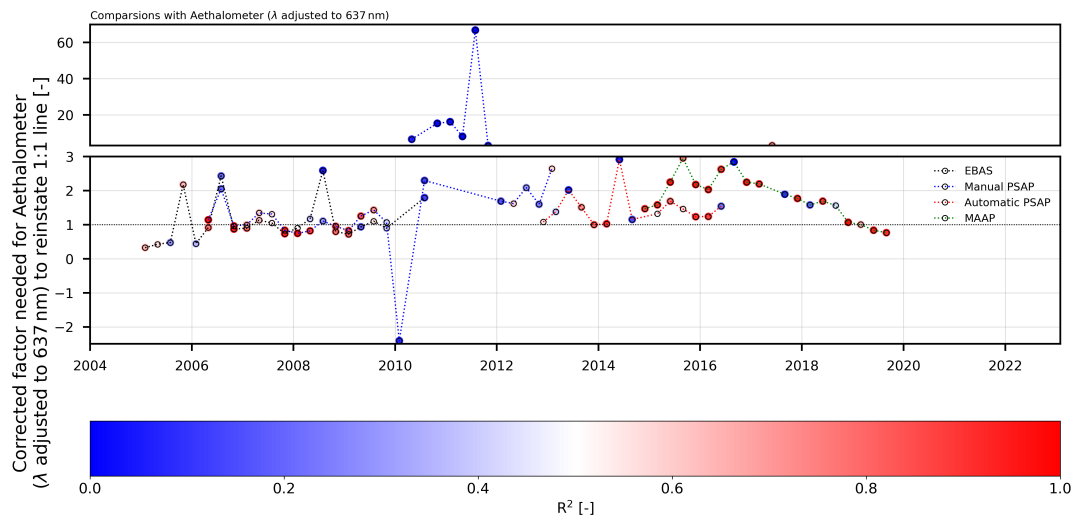


Figure S3. Comparisons between with absorption coefficient (σ_{ap}) from the Aethalometer (A31) and σ_{ap} from the three instruments/data sets EBAS (black), Manual Particle Soot Absorption Photometer (PSAP) (blue), automatic PSAP (red), and Multi-Angle Absorption Photometer (MAAP) (green). Note that EBAS represents the σ_{ap} from the same custom-built PSAP however different pre-processing has been performed on the data. The data from the different instruments are compared with one another to ascertain the coefficient of regression (using the Theil Sen Slope). The reciprocal is the correction factor (CF). Comparisons are done every 3-month intervals. Only comparisons where there were at least 50 data points are shown. The CF is the ratio of the σ_{ap} from either the EBAS database (black), Manual PSAP (blue), Automatic PSAP (red), and MAAP (green), compared with the σ_{ap} from the AE31. All σ_{ap} are adjusted to 637 nm. Furthermore, the data points are coloured based on their respective R^2 values for each respective comparison.

S2.4 Absorption Ångström Exponent (derived from Aethalometer)

Absorption Ångström exponent represents the wavelength dependence of the aerosol absorption coefficient (σ_{ap}). This intensive aerosol optical property depends on aerosol composition, so different aerosol types have unique ranges of AAE values. AAE is computed using the following equation:

$$85 \quad AAE = -\frac{\log(\sigma_{a1}) - \log(\sigma_{a2})}{\log(\lambda_1) - \log(\lambda_2)} \quad (S.4)$$

For figure S4, the Ångström Absorption Exponent (AAE) was calculated using all the wavelengths available (i.e. 370, 470, 520, 590, 660, 880, 950 nm). The absorption coefficients for multiple wavelengths are provided up the Aethalometer at Zepelin. We used the line of best fit for $\ln(\sigma_{ap})$ vs. $\ln(\lambda)$, for all wavelengths and coefficients i.e. 370, 470, 520, 590, 660, 880, 950 nm, to calculate the AAE.

- 90 Figure S4, displays the trend in the Ångström Absorption Exponent from 2005 to 2020, consisting of 15 years. The trend calculated with the 3pw method, is 0.0005 yr^{-1} . The AAE decreases from 0.785 to 0.777. Using the equation S.2 with 0.78 as opposed to 1, leads to an adjustment of 0.86 as opposed to 0.82, if we use the wavelengths 525 and 637. The factor that scales the absorption coefficient changes from $0.85^1 = 0.82$ to $0.85^{0.785} = 0.86$ or $0.85^{0.777} = 0.86$. Hence the absorption coefficient would be 1.04 greater using the AAE of 0.777-0.785 as opposed to 1. The use of this adjustment (i.e. AAE = 0.78-0.79)
- 95 should only be used for the period when the conversion between the wavelengths is used i.e. before the introduction of the MAAP. Hence, for simplicity, an AAE = 1 is used in the paper.

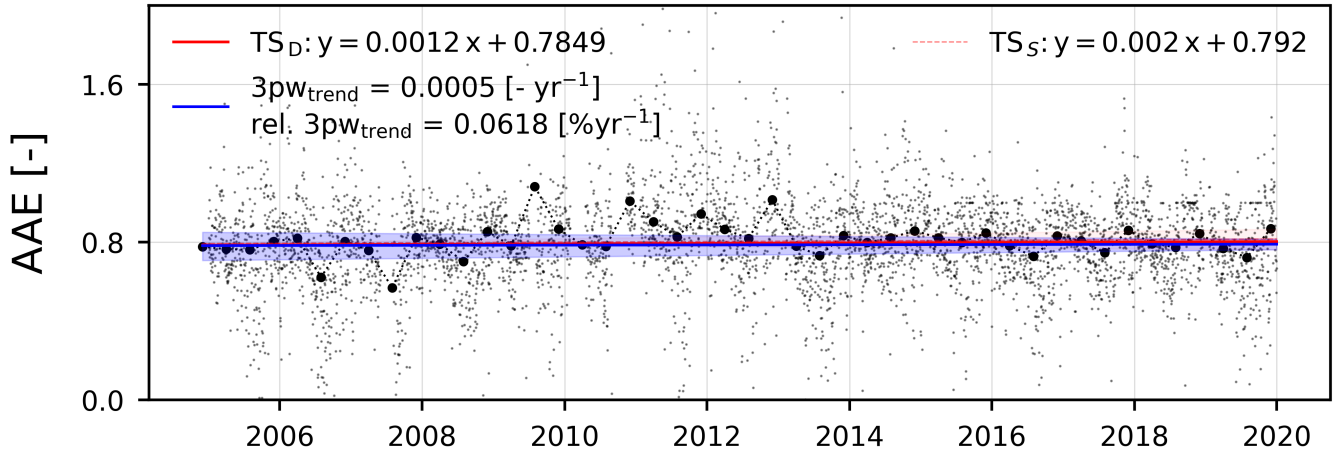


Figure S4. The trend in the Ångström absorption coefficient (AAE) from 2011 to 2020, based on the AAE generated using all the available wavelengths. The trends are provided based on seasonal medians (T_S), and daily medians (T_D), the 3pw method is also used on the daily medians and the trend is stated.

S2.5 Nephelometer comparison: TSI vs. Ecotech

For harmonisation, the TSI nephelometer was used as the reference instrument. The scattering coefficient (σ_{sp}) hourly arithmetic mean values of the Ecotech nephelometer were compared with the hourly means σ_{sp} for the TSI. The two data sets were temporally collocated to perform the comparison. For the comparison, TSI σ_{sp} measurements at wavelengths 550 and 700 were adjusted to 525 and 635 nm and the wavelengths 525 and 635 of Ecotech σ_{sp} values were adjusted to 550 and 700 nm, using equation S.5 and S.2. Equation S.2, is used to adjust σ_{sp} to any other wavelength λ_x , see Müller et al. (2011) for further details. For wavelength adjustment, the scattering Ångström exponent (SAE) is computed from the blue (450 nm) and green (550 nm) wavelengths.

$$105 \quad \text{SAE} = -\frac{\log(\sigma_{sp}^{\lambda_1}/\sigma_{sp}^{\lambda_2})}{\log(\lambda_1/\lambda_2)} \quad (\text{S.5})$$

For the adjustment of the scattering coefficient, AAE in equation S.2 is substituted as the Scattering Ångström Exponent (SAE).

The Ecotech typically overestimates the scattering coefficients when compared to the TSI. The correction factors applied to the Ecotech σ_{sp} means are follows for wavelengths 450, 525, 530, 550, 635, 637 and 700 are as follows: 0.93, 0.90, 0.90, 0.92, 1.03, 1.03 and 1.11.

The correction factors are applied to the σ_{sp} values of the Ecotech, in order to correct for any systemic biases (i.e. match the TSI). The overlap of available data is only 2 months. It should be noted that there were additional problems with the TSI from 2016 onwards. The problems with the TSI were likely caused by the instrument being stuck in the zeroing mode, which is when the light scattered by the carrier gas, the instrument walls and the background noise in the detector is measured. The problem was dealt with by taking only the measurements where the instrument was considered not to be in the zeroing operation mode. This procedure was able to be performed and the data were cleaned as it was found that these normal modes of operation had a recurring pattern.

SSA is given in terms of wavelength 637 nm, hence the TSI and Ecotech σ_{sp} are adjusted to 637 nm after the correction factors are applied to the Ecotech σ_{sp} values.

120 S3 Collocating ERA5 and HYSPLIT

In Fig. S5, we compare the two accumulated surface precipitation along the back trajectories (ATP) time series. The idea here was to create a continuous data set for ATP and to account for the discontinuity between shifting from the FNL to the GDAS meteorological fields at the end of 2004. The two time series correspond well with one another, however, it is noticeable that for the FNL period (2002 - 2004) they do not compare as well. Later on, after 2021 the ERA5 ATP is substantially greater than the GDAS ATP. As part of the ERA5 data, the resolution for ATP is much finer, compared with the GDAS which provides precipitation rates per 0.1 mm.

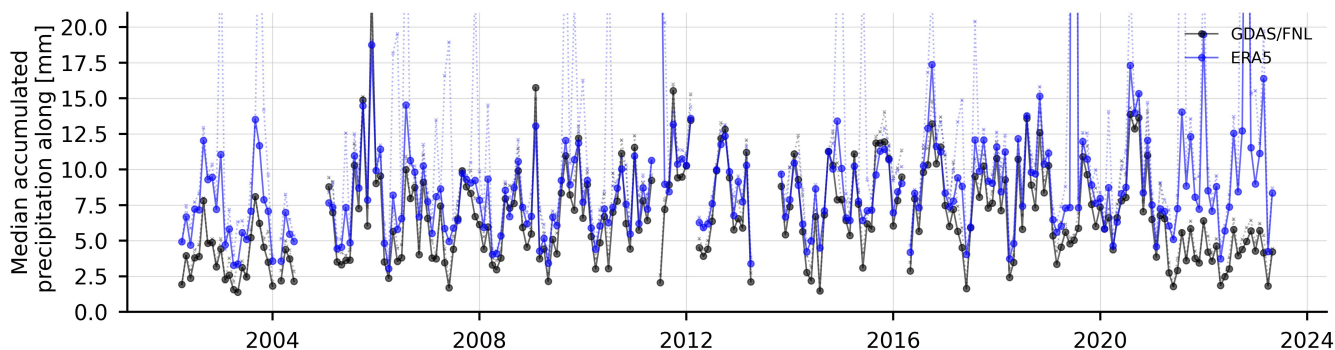


Figure S5. The monthly median values for the accumulated surface precipitation along the back trajectories (ATP) is displayed for the HYSPLIT output which is based on the FNL (Final) Operational Global Analysis archive data from The National Weather Service's National Centers for Environmental Prediction (NCEP) and the Global Data Assimilation System (GDAS) meteorological fields (black lines), and for the temporarily and spatially collocated fifth generation ECMWF atmospheric reanalysis of the global climate (ERA5) surface precipitation data (blue lines).

S4 Assigning clusters

Five clusters, representing different transportation pathways were determined via the k-means clustering method. The 27-size ensemble was simplified such that only one cluster was assigned to every hourly observation. Hence, to classify the arriving air masses, we decided to remove ensembles that contained a mix of clusters. It was decided that the cluster we assign to the hourly value would need to represent at least 50% of the 27-ensemble (i.e. be assigned to at least 14 back trajectories out of a possible 27, as part of the arriving ensemble of back trajectories). See Fig. S6 for the breakdown of the counts per maximum fraction of the contributing clusters (i.e. the assigning cluster). The threshold for the largest fraction of the contributing cluster was 0.5, meaning that if the largest fraction for any of the 5 clusters was less than 0.5, then no cluster would be assigned to that particular hourly value.

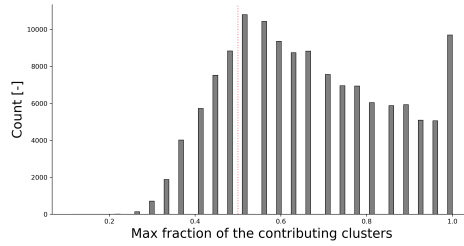


Figure S6. Frequency plot for the maximum proportion of one particular cluster for a given observation. For an ensemble of 27 back trajectories the majority of observations were tied to one or more back trajectory clusters, hence values below 1. If the observation had almost equal contribution from all clusters (i.e. $\sim 5/27$ would be the maximum fraction for this)

S5 Active fires derived from MODIS

In order to count the number of active fires downwind of ZEP, MODIS Satellite data was utilised along with the back trajectories. For each $1^\circ \times 1^\circ$ grid, the number of active fires present in the grid cell was summed up. By gridding the MODIS data, the calculations became easier and a rough spatial allowance was given to the endpoints of the back trajectories (i.e. the back trajectories did not have to exactly traverse over the coordinates of the fire). For each and every 10-day back trajectory, the sum of active fires within each grid cell traversed was added up, providing an active fire count.

Time interval for back traj. (within ML): 2002-07-18 17:00:00 - 2002-07-09 02:00:00
Time interval for MODIS fire data: 2002-07-09 - 2002-07-18
Ensemble of Trajs pass through: 381.0 active fires in 24 hrs.

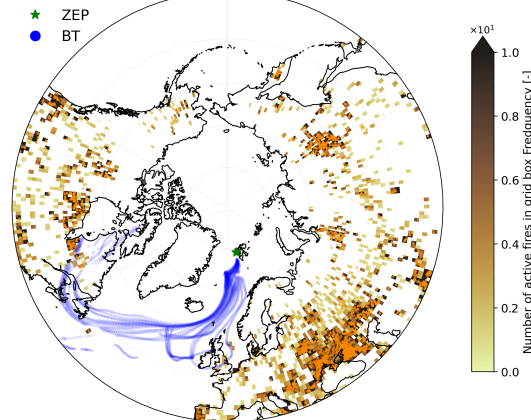


Figure S7. Example plot showing how the active count along the back trajectories is calculated: a back trajectory arriving at Zeppelin Observatory 01:00:00 on the 19th of July 2002 is displayed (blue). The active forest fires, for that period in which the back trajectory is present, are displayed as orange triangles. The number of active fires within each grid cell is counted. The colours of the grid cells correspond to the number of active fires per grid call; this is displayed by the colour bar. All active fire data is taken from NASA satellite products, and in particular the MODIS Satellite (<https://firms.modaps.eosdis.nasa.gov/download/>). The number of active fires that each back trajectory traverses over whilst in the mixed-layer is counted. The sum for an ensemble of back trajectories for a particular arrival time is added together. In this example, for this given timestamp, grids were traversed containing a total of 384 active fires.

S6 Trend analysis since 2016

We focus here on the period after which we observe a local minimum in the absorption coefficient time series. Figure S8, represents the trend after 2015. We observe an increasing tendency in the absorption coefficient in the Arctic Haze season (AHZ). The increase in the AHZ season from 2016 onwards, according to the 3pw method, is statistically significant and corresponds to about $3\% \text{yr}^{-1}$. The AHZ is the only season, from 2016 onwards, which displays a s.s. tendency; summer (SUM) and the slow build-up season (SBU) correspond to $1.2\% \text{yr}^{-1}$ and $0.7\% \text{yr}^{-1}$ respectively. It is important to remember that the detection of reliable trends depends on the length of the time series and on the magnitude of the slope, due to the potential errors/artefacts of the method for too short time series, which can lead to too high absolute slopes and also the strong influence of beginning and end years. Collaud Coen et al. (2020) recommends at least 10 years but also uses some 9-year time series. Here, we choose to fit essentially two ramps, after a local minimum, a method widely used in parametric trend analysis. If we were to impose the same requirement and hence, focus on the last 10 and 9 years of data i.e. (2014/2015 -2023, we would observe a non-s.s. tendency of $0.83\% \text{yr}^{-1}$ and $1.2\% \text{yr}^{-1}$ respectively for the AHZ season.

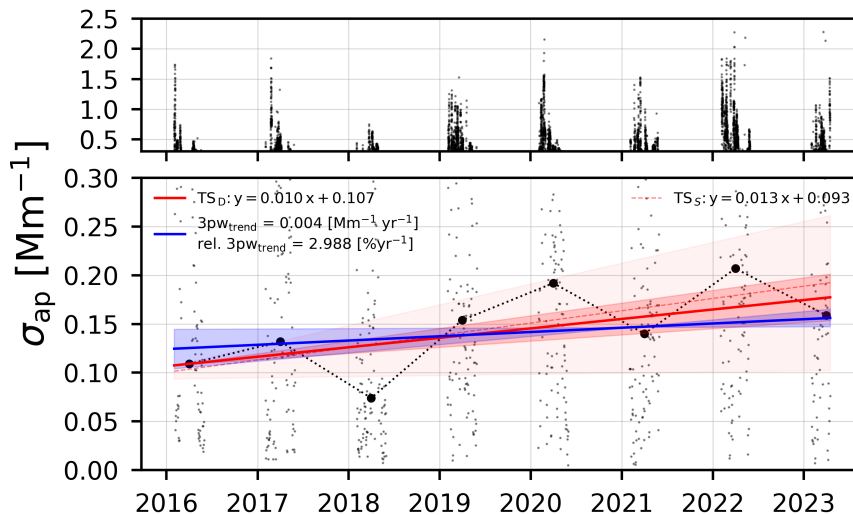


Figure S8. Multi Angle Absorption Photometer (MAAP) time series for the absorption coefficient (σ_{ap}) measured at Zeppelin observatory for the last 8 full years of data (2016-2023). The Theil-Sen Slope (TS) trend line is displayed as a dashed red line with a red-shaded region corresponding to 95% significance. The trend lines are both calculated using the seasonal medians (TS_S), and daily medians (TS_D). The 3pw method is used to apply a trend shown in blue, the intercept is calculated using the median value halfway through the time series. The relative trend for the 3pw is calculated by dividing the absolute trend by the AHZ median for the time series at hand.

S6.1 Single scattering albedo

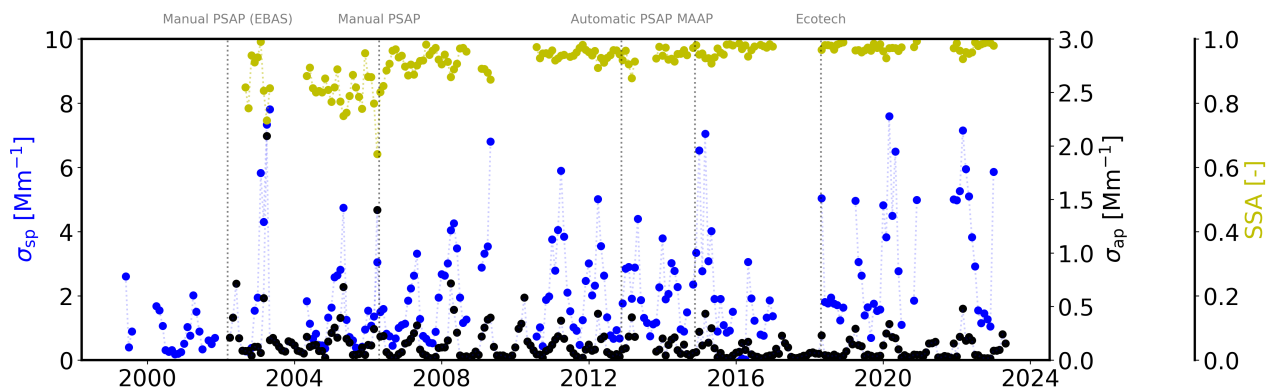


Figure S9. Time series for the harmonised absorption coefficient (σ_{ap} at 637 nm), the scattering coefficient (σ_{sp} at 637 nm), and the single scattering albedo (SSA) i.e. $\sigma_{sp}/(\sigma_{sp} + \sigma_{ap})$.

155 S7 Concentration weighted trajectory mappings

Figure S10, displays the spatial variation in the CWT σ_{ap} value. The largest contributions come from Eurasia. To demonstrate the validity of the CWT, it is also worth noting the various forest fire events, in particular the fire in May 2006 in Eastern

Europe that was effectively transported to the Arctic (Stohl et al., 2007), and the fire during the 10-17th of July 2015 in the Yukon-Koyukuk state of Alaska (Markowicz et al., 2016), appear in their respective annual CWT mappings.

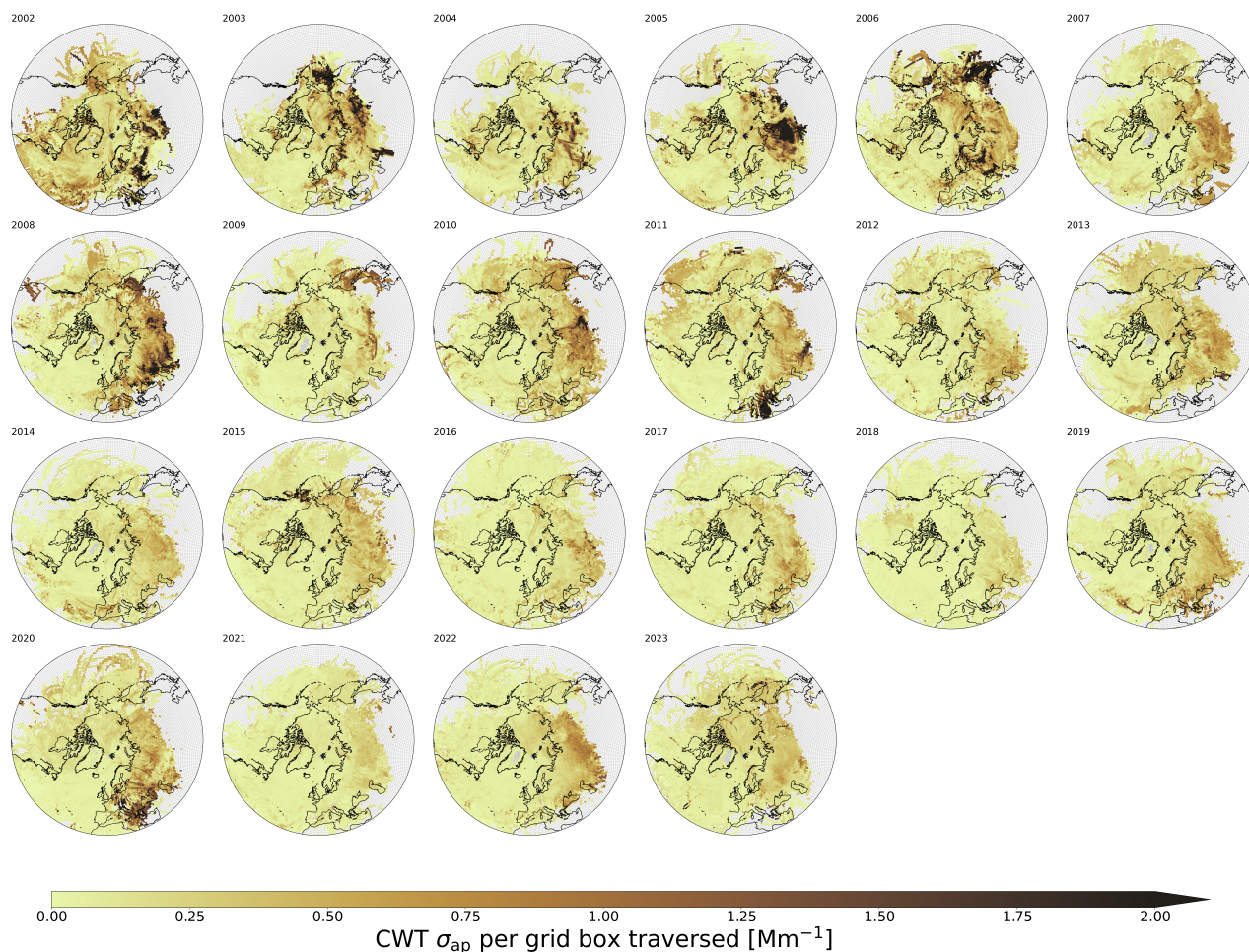


Figure S10. Concentration Weighted Trajectory (CWT) mappings from 2002 - 2023: CWT values for σ_{ap} for each year of data from 2002 to 2023 are calculated according to Hsu et al. (2003).

160 S8 Trends in ECLIPSE V6b global emission fields

The figure, S11 uses the emission inventories from the ECLIPSE V6b global emission fields for 2000, 2005, 2010, 2015 and 2020 to calculate the trend for each grid cell. The majority of regions display decreasing trends for those emission inventory data sets. However, parts of the Middle East, Central Asia and North Africa exhibit increasing trends. Spatial changes in the ECLIPSE emissions inventories can also be found in AMAP (2021).

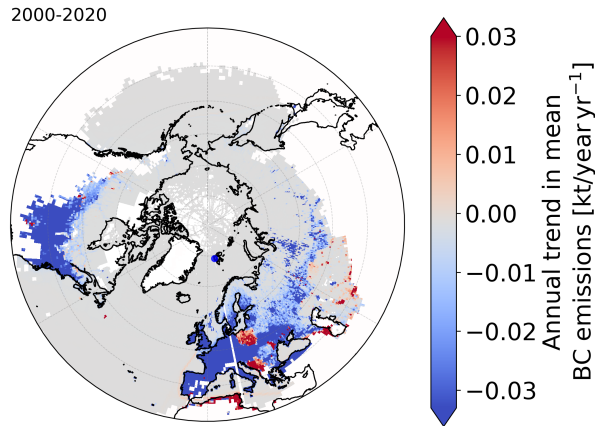


Figure S11. Spatial trend for the BC emissions per a grid cell for the ECLIPSE V6b global emission fields for 2000, 2005, 2010, 2015 and 2020. The map is masked based on the spatial coverage of the HYSPLIT endpoints, to ensure a like-for-like comparison of the same grid cells.

165 S9 Annual frequency of five clusters

The annual cycle for the five clusters is composed of the data between 2002 and 2023. The North Atlantic cluster is more dominant during the summer months, whilst Siberia and Eurasia contribute relatively more during the winter, signifying the timing of the Arctic Haze (see Fig. S12).

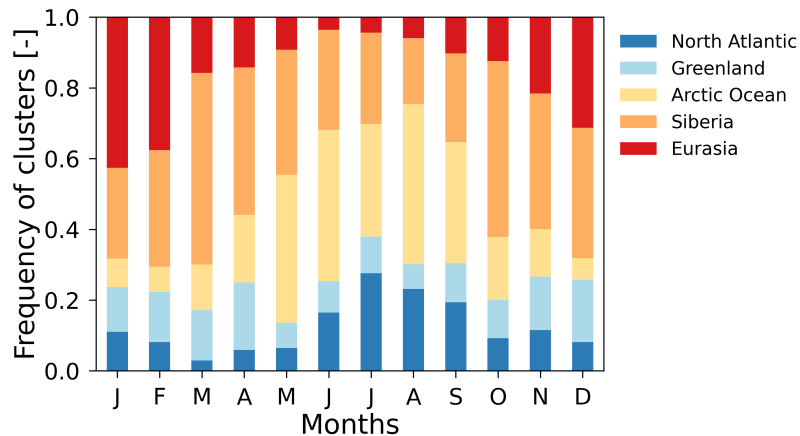


Figure S12. The normalised proportion of the various air mass clusters for each month: Each cluster is signified by a different colour: North Atlantic (blue), Greenland (light blue), Arctic Ocean (yellow), Siberia (orange), and Eurasia (red). Each month is normalised by the total number of occurrences for that particular month. The simplified data set is displayed, which means that the 14 back trajectory requirement (i.e. 50% of the 27-ensemble for the most frequent back trajectory) has been placed on the data set.

S10 Cluster trends

170 The Eurasian cluster i.e. 5 is the only cluster that displays a positive long-term relative 3pw trend (see Figs.S13 b), c) and d)). The Arctic Haze trend is negative, whilst SUM and SBU display positive relative 3pw trends. For the Eurasian cluster, the combined trend exhibits a positive relative 3pw trend of $0.110\% \text{yr}^{-1}$ and is homogeneous and s.s. at a confidence level of 36%.

The North Atlantic Cluster (1), displays negative trends in the absorption coefficient (σ_{ap}) for all seasons with a statistically significant trend in the slow-build-up season (SBU). The trends are homogeneous and s.s. for all seasons at the confidence level of 47%. The Greenland cluster exhibits s.s. decreasing trends in summer (SUM) and SBU, with a homogeneous and s.s. for all seasons at the confidence level of 22%. The Arctic Ocean displays decreasing trends, SUM displaying a s.s. trend. The combined trend for all seasons for the AO cluster is homogeneous and s.s. at 4%. The Siberian cluster displays decreasing trends for all seasons, with the combined trend homogeneous and s.s. at 80%.

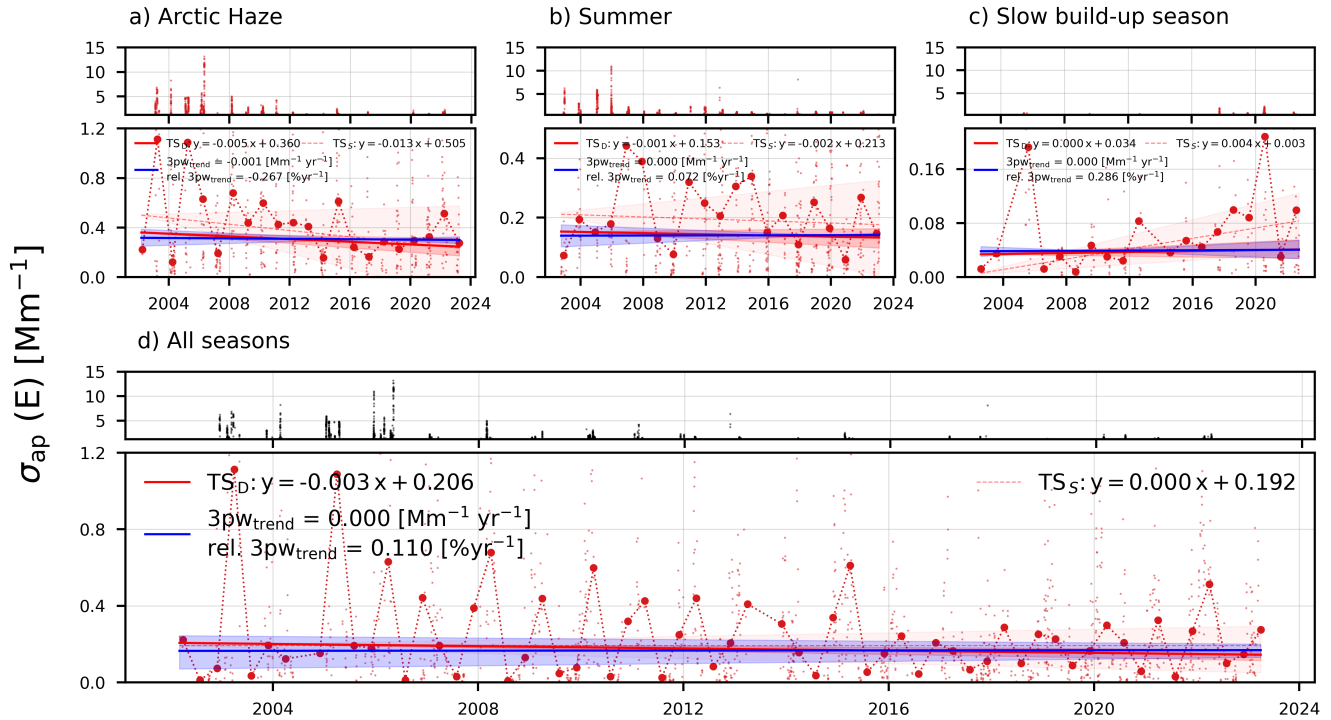


Figure S13. The time series for σ_{ap} for the Eurasian cluster. The trend analysis is performed on seasonal (TS_S) and daily resolutions (TS_D), the prewhitened trend using the 3pw method on the daily medians is also included, along with the relative trend (i.e. 3pw trend divided by the median). Cluster analysis was performed using the latitude, longitude and altitude of all data points in the collocated data set. The length of each back trajectory was set at 10 days. The trends for subplots a), b) and c) are the following a) Arctic Haze: $\text{TS}_D = -0.005x + 0.360$, $\text{TS}_S = -0.013x + 0.505$, with $3\text{pw}_{\text{trend}} = -0.001 \text{ Mm}^{-1} \text{ yr}^{-1}$ & relative $3\text{pw}_{\text{trend}} = -0.267 \text{ \%yr}^{-1}$, b) Summer: $\text{TS}_D = -0.001x + 0.153$, $\text{TS}_S = -0.002x + 0.213$, with $3\text{pw}_{\text{trend}} = 0.000 \text{ Mm}^{-1} \text{ yr}^{-1}$ & relative $3\text{pw}_{\text{trend}} = 0.072 \text{ \%yr}^{-1}$, and c) Slow build-up: $\text{TS}_D = 0.000x + 0.034$, $\text{TS}_S = 0.004x + 0.003$, with $3\text{pw}_{\text{trend}} = 0.000 \text{ Mm}^{-1} \text{ yr}^{-1}$ & relative $3\text{pw}_{\text{trend}} = 0.286 \text{ \%yr}^{-1}$.

S11 Seasonality

180 From figure S14 the accumulated BC emissions display a peak in winter (DJF). The median absorption coefficient displays a peak in March (M), corresponding to the typical Arctic Haze in late winter-early spring. The difference in the peak of

185 BC emissions i.e. DJF and the peak in σ_{ap} in February - April, can be argued to be caused by the changing meteorological conditions, which can be seen in the reduction in ATP in from March to May. The source regions change, i.e. more from Eurasia and Siberia and less from the North Atlantic, thus ATP decreases (AHZ). The slight dip in the sink effect brought about by a decline in ATP from March to May (MAM), helps explain the distinct Arctic aerosol seasonality.

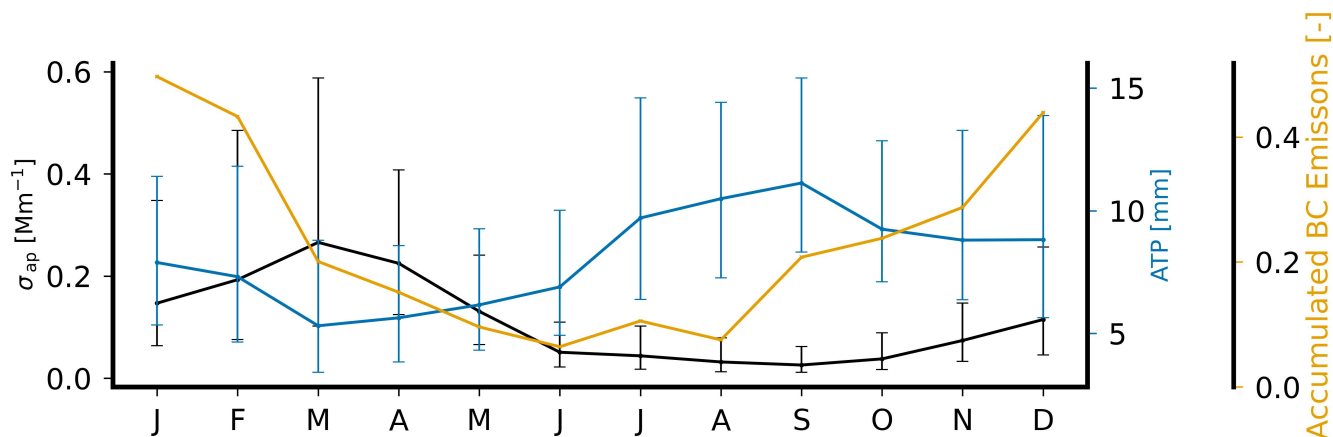


Figure S14. Seasonality plots for the measured absorption coefficient, σ_{ap} , (black), the accumulated back trajectory precipitation (ATP) (blue) and the accumulated emission of BC on the back trajectories, based on emission inventories from ECLIPSE (yellow). The absorption coefficient and ATP show monthly median values with the error bars displaying the 25th and 75th percentiles.

S12 Extreme values

Using a 15 day rolling 99th a threshold was defined for each day of the year. The threshold was used to establish for each hourly data point whether or not it should be considered an extreme value. Hourly values above the corresponding threshold for that day of the year were considered extreme and values below the threshold were considered non-extreme. The full-time series
 190 (i.e. 2002 - 2023) for the variables accumulated back trajectory precipitation and emissions of BC from fires were utilised to define the extreme value thresholds for each day of the year.

S12.1 Extremely high ATP

Clean days correspond with the lowest 1st percentile of absorption coefficient (σ_{ap}). We observe that 18 % of the “clean” days at ZEP, coincident with back trajectories which have experienced extremely high amounts of accumulated precipitation (i.e.
 195 “wet” conditions). We also observe that the proportion of clean days that coincident with extremely high ATP back trajectories has increased in the past 22 years.

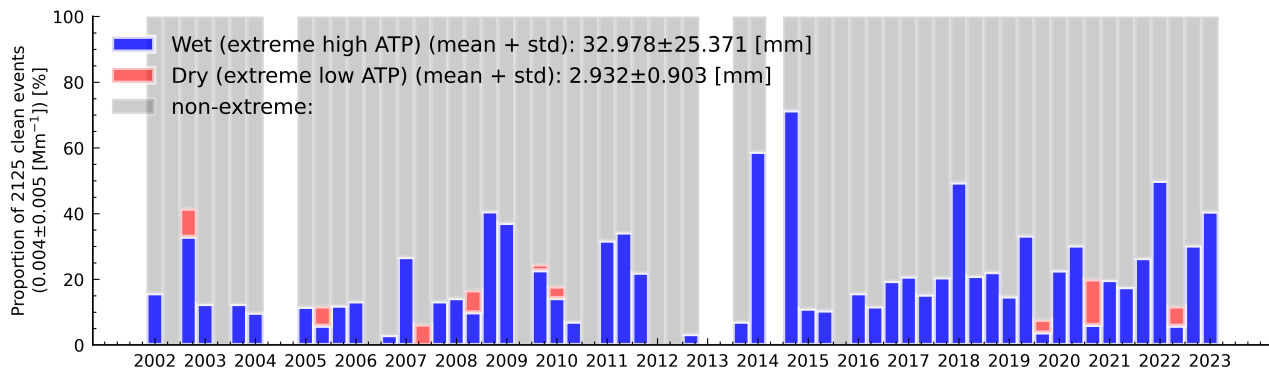


Figure S15. Proportion of clean days connected to extremely high accumulated back trajectory precipitation (ATP), extremely low ATP and neither. The data is split into seasons (i.e. AHZ, SUM, SBU). The proportion of the clean days (using the lowest 1% of σ_{ap} data) coinciding with either wet events (99th percentile of ATP) and dry events (1st percentile of ATP).

S12.2 Impact of active fires:

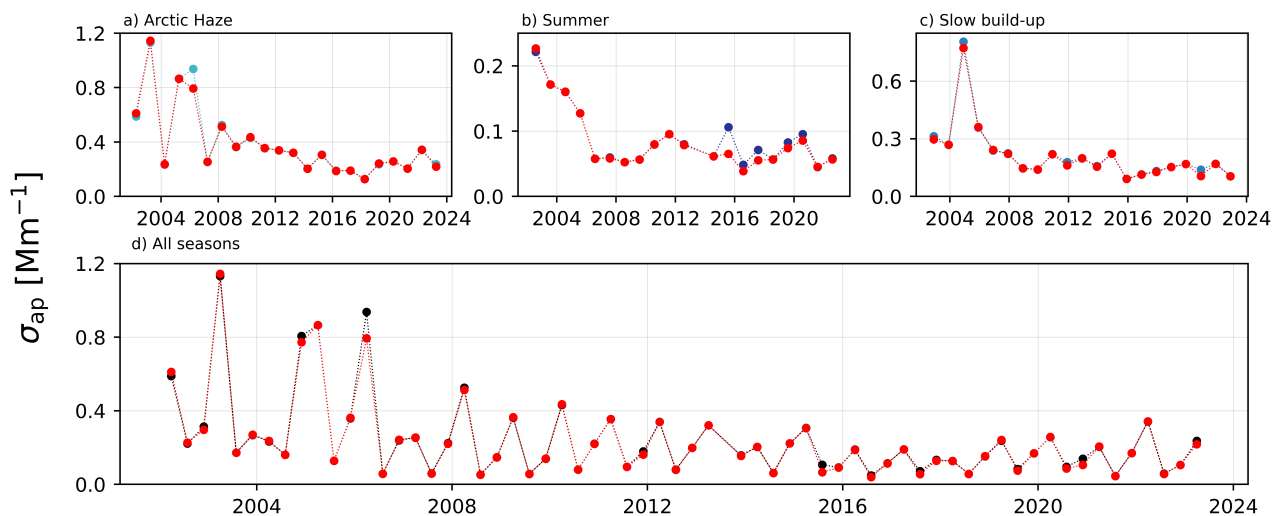


Figure S16. Time series of arithmetic absorption coefficient values for the removal and inclusion of extreme biomass burning events: Extreme biomass burning (BB) events were categorised as such using a 15-day 99th running percentile, of the accumulated BC emissions along back trajectories (according to GFED), to construct a threshold for each day of the year. The day of the year threshold was then applied to the whole time series. The events were categorised as extreme BB events if the hourly values surpassed the threshold for that day of the year. The time periods in which extreme biomass burning (BB) events are included (i.e. all data present) are given in various colours depending on the season. The red data points signify the removal of the extreme BB events from the time series. Seasonal arithmetic means are calculated for a) Arctic Haze season, b) Summer season, and c) Slow build-up season and d) the entire time series. For the summer season, it is noticeable how the removal of these extreme events has lowered the seasonal arithmetic mean, especially in 2015.

S13 Example of ATP- σ_{ap} relationships for the calculated absorption coefficient

As part of the method for trying to ascertain the influence of accumulated back trajectory precipitation (ATP) on the long-term absorption coefficient (σ_{ap}) trends, the site-specific relationship between ATP and σ_{ap} was investigated. For each cluster and season, the relationship between σ_{ap} and ATP is examined. It is important to note that these relationships between the σ_{ap} and ATP are unique to the receptor (i.e. ZEP).

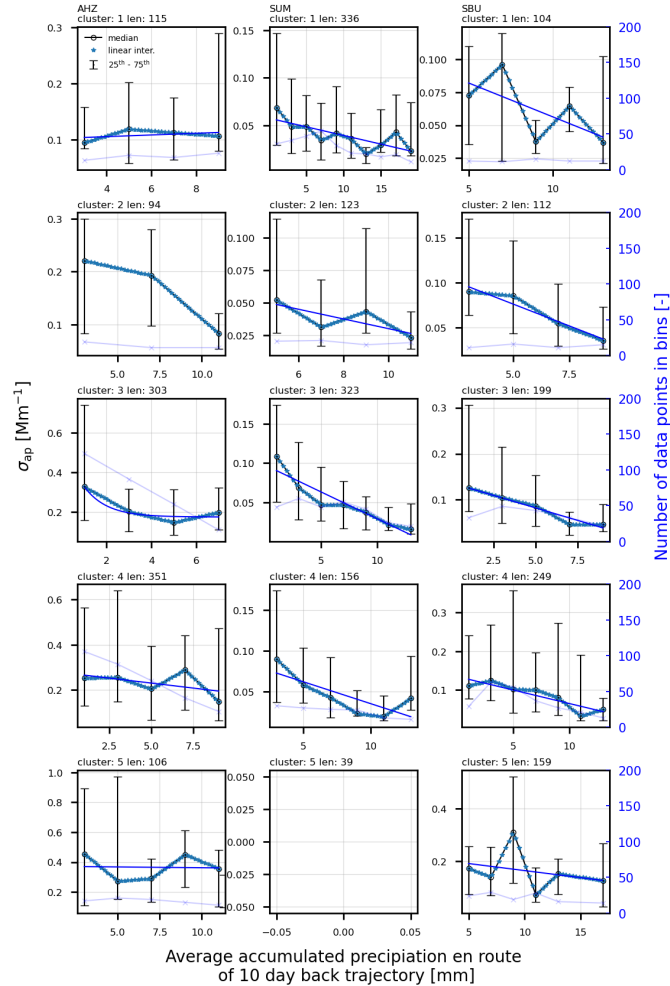


Figure S17. Example of an ATP- σ_{ap} relationship. The data for each subplot is composed of temporally collocated hourly averages of ATP and σ_{ap} . The data is binned using a 2 mm interval. The fraction of data used for the sub-sample is 0.5. A threshold of 10 data points is required for each bin. The median for each bin is then linearly interpolated to achieve a better resolution.

The season and cluster-specific relationships (see Fig.S17) are used to map the ATP long-term trend onto calculated absorption coefficient values ($\sigma_{ap,cal.}$). After the mapping, the trend of the calculated values is calculated using the 3pw method. The seasonality is well captured by $\sigma_{ap,cal.}$. It is important to note that figure S17 simply serves as an example; this method was performed multiple times, varying the bins and the fraction of data used, and each time calculating the trend in $\sigma_{ap,cal.}$.

References

- AMAP: Impacts of short-lived climate forcers on Arctic climate, air quality, and human health, Arctic Monitoring and Assessment Programme (AMAP), 2021.
- 210 Bond, T. C., Anderson, T. L., and Campbell, D.: Calibration and intercomparison of filter-based measurements of visible light absorption by aerosols, *Aerosol Science & Technology*, 30, 582–600, 1999.
- Collaud Coen, M., Andrews, E., Alastuey, A., Arsov, T. P., Backman, J., Brem, B. T., Bukowiecki, N., Couret, C., Eleftheriadis, K., Flentje, H., et al.: Multidecadal trend analysis of in situ aerosol radiative properties around the world, *Atmospheric Chemistry and Physics*, 20, 8867–8908, 2020.
- 215 Hsu, Y.-K., Holsen, T. M., and Hopke, P. K.: Comparison of hybrid receptor models to locate PCB sources in Chicago, *Atmospheric environment*, 37, 545–562, 2003.
- Hulst, H. C. and van de Hulst, H. C.: *Light scattering by small particles*, Courier Corporation, 1981.
- Markowicz, K. M., Pakszys, P., Ritter, C., Zielinski, T., Udisti, R., Cappelletti, D., Mazzola, M., Shiobara, M., Xian, P., Zawadzka, O., et al.: Impact of North American intense fires on aerosol optical properties measured over the European Arctic in July 2015, *Journal of Geophysical Research: Atmospheres*, 121, 14–487, 2016.
- 220 Müller, T., Laborde, M., Kassell, G., and Wiedensohler, A.: Design and performance of a three-wavelength LED-based total scatter and backscatter integrating nephelometer, *Atmospheric Measurement Techniques*, 4, 1291–1303, 2011.
- Ogren, J. A.: Comment on “Calibration and intercomparison of filter-based measurements of visible light absorption by aerosols”, *Aerosol Science and Technology*, 44, 589–591, 2010.
- 225 Stohl, A., Berg, T., Burkhardt, J., Fjærå, A., Forster, C., Herber, A., Hov, Ø., Lunder, C., McMillan, W., Oltmans, S., et al.: Arctic smoke-record high air pollution levels in the European Arctic due to agricultural fires in Eastern Europe in spring 2006, *Atmospheric Chemistry and Physics*, 7, 511–534, 2007.
- Virkkula, A.: Correction of the calibration of the 3-wavelength Particle Soot Absorption Photometer (3λ PSAP), *Aerosol Science and Technology*, 44, 706–712, 2010.
- 230 Zieger, P., Fierz-Schmidhauser, R., Gysel, M., Ström, J., Henne, S., Yttri, K. E., Baltensperger, U., and Weingartner, E.: Effects of relative humidity on aerosol light scattering in the Arctic, *Atmospheric Chemistry and Physics*, 10, 3875–3890, 2010.